Molecular Dynamics Study of Dendrimer Molecules in Solvents of Varying Quality

Michael Murat[†] and Gary S. Grest[*,‡]

Soreq Nuclear Research Center, Yavne 81800, Israel, and Corporate Research Science Laboratories, Exxon Research and Engineering Company, Annandale, New Jersey 08801

Received August 21, 1995; Revised Manuscript Received November 8, 1995[⊗]

ABSTRACT: The properties of dendrimers ("starburst" molecules) under varying solvent conditions are studied using molecular dynamics simulations. The dendrimers are found to have a compact (space filling) structure under all solvent conditions, with a radius of gyration which scales with the number of monomers as $R_G \propto N^{1/3}$. For high generation number dendrimers, there is a distinct region of constant monomer density. The density in this region depends only on the solvent quality and is independent of the generation number. When the contributions of the different generations to the overall density profile are separated, we find that the monomers which belong to the first few generations are stretched and spatially localized. Later generations are less localized and penetrate well into the central regions of the dendrimer. The different primary branches ("dendrons") of the dendrimers are found to be segregated. The amount of spatial overlap between the different dendrons decreases with increasing generation number of the dendrimer and increasing solvent quality. The relaxation times of the fluctuations of the internal structure were evaluated as well, to ensure that the simulations were run long enough for adequate sampling.

I. Introduction

A special class of branched polymers is the dendrimers or "starburst" molecules. These molecules consist of relatively short chains with multifunctional groups at both ends. When built around an initiator core, with the functional groups of each generation reacted before adding a new generation, these chains form molecules that resemble a Cayley tree.[1,2] Dendrimers are characterized by the number of generations g they contain, the functionality b of the end groups, and the number of monomer segments n between the functional groups (the spacer). The total number of monomers a dendrimer contains grows exponentially with its generation number and is given by $N = nb[(b - 1)^{g+1} - 1]$. Obviously, as the volume that is available to the dendrimers grows only as g^3, the dendrimers cannot be grown indefinitely. A schematic diagram of such dendrimers with trifunctional end groups is shown in Figure 1. For a recent review of a variety of synthetic routes for producing dendrimers, see Voit.[2]

An early attempt to analyze the structure of dendrimers was made by de Gennes and Hervet.[3] Their self-consistent field analysis was for dendrimers with long spacers (large n). Assuming that the monomers of each generation lie in a concentric shell of their own, they concluded that a perfect dendrimer can be grown up to a limiting generation number $g_l \simeq 2.88(\ln n + 1.5)$. Up to that generation number, the concentration profile of dendrimers grows parabolically near the core and saturates at a value of order 1 at the outer regions. They found that the size of the dendrimer depends on the number of monomers as $R \propto N^{1/5}$, giving an effective fractal dimensionality $d_f = 5$. Beyond the limiting generation number, only imperfect growth is possible, with some of the end groups being only bifunctional. Naylor *et al.*[4] carried out atomic-scale molecular dynamics (MD) simulations of dendrimers up to generation

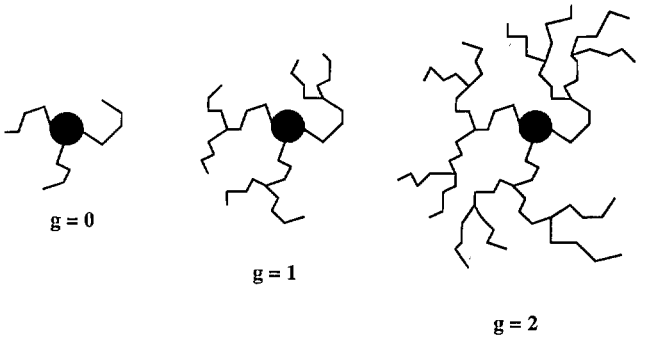

Figure 1. Schematic diagram of a dendrimer with $b = 3$ and $n = 4$. Generation numbers $g = 0$, 1, and 2 are shown. The inner circle represents the core.

7. These simulations used atomic-level force fields and consequently yield detailed information on the molecular structures. However, since the relaxation times of polymeric molecules are extremely long, it is not clear if the structures obtained in these simulations are thermodynamically equilibrated. Nevertheless, the visualizations of the simulated dendrimers show rather open structures, with no indications of the concentric shell structure assumed by de Gennes and Hervet. The first simulations of course-grained models of dendrimers were performed by Lescanec and Muthukumar,[5] who built dendrimers by an off-lattice kinetic growth algorithm of self-avoiding walks. In contrast to the results of de Gennes and Hervet,[3] they found a density profile that decreases monotonically outward from the center of the molecule. The simulations exhibited significant chain folding. The dendrimer size was found to scale with the number of monomers and the spacer length as $R \propto N^{\nu}n^{\beta}$, with $\nu = 0.22 \pm 0.02$ and $\beta = 0.50 \pm 0.02$. The N dependence is in accordance with the self-consistent field results. However, no thermodynamic relaxation was performed on the kinetically grown structures, and it is not clear whether these results hold for equilibrated dendrimers. Mansfield and Klushin[6] later showed that the hydrodynamic radii calculated using the Lescanec−Muthukumar structure is consistent with the experimental hydrodynamic radii. The

* To whom correspondence should be addressed.
† Soreq Nuclear Research Center.
‡ Exxon Research and Engineering Company.
⊗ Abstract published in *Advance ACS Abstracts,* January 1, 1996.

0024-9297/96/2229-1278$12.00/0

same authors performed Monte Carlo simulations of dendrimers and found[7] a density profile qualitatively similar to the one found in ref 5, except that the density profile exhibits a minimum as a function of the distance from the center for high generation numbers. Their simulations showed that the chains are folded to an extent that the monomers of the terminal generation are found at all distances from the center of the dendrimer. A detailed analysis of these simulations[8] demonstrated that the different dendrons (the different branches at the first level of branching) demix and segregate even though the monomers are chemically identical. In addition to simulations, renormalization group methods have also been applied to study dendrites in good solvent conditions.[9]

For all these studies the dendrimers were in a very good solvent. In this paper, we present molecular dynamics simulations of dendrimers in solvents of varying quality. To our knowledge, these are the first simulations of dendrimers that incorporate solvent effects. In the next section, we describe the simulation model and method. The results are presented in section III. In section IV, we briefly summarize our main conclusions.

II. Simulation Model and Method

We simulate the dendrimer molecules using a molecular dynamics method, solving Newton's equation of motion of each monomer. We treat the solvent as a continuum, which acts as a heat bath for the dendrimer and produces a viscous drag when the dendrimer moves. The equation of motion for monomer i of mass m is thus given by

$$m\frac{d^2\vec{r}_i}{dt^2} = -\vec{\nabla}U_i - m\Gamma\frac{d\vec{r}_i}{dt} + \vec{W}_i(t) \tag{1}$$

where Γ is the friction coefficient that couples the monomers to the heat bath. The random part of the monomer-heat bath coupling is given by a white-noise term $\vec{W}_i(t)$, which satisfies

$$\langle\vec{W}_i(t)\cdot\vec{W}_j(t')\rangle = 6k_BTm\Gamma\delta_{ij}\delta(t-t') \tag{2}$$

Here k_B is the Boltzmann constant and T is the temperature. The potential U_i is composed of two terms: $U_i = \sum_j U_{ij}^0 + U^{ch}$. U_{ij}^0 is a Lennard-Jones (LJ) potential

$$U_{ij}^0(r) = \begin{cases} 4\epsilon\left[\left(\frac{\sigma}{r}\right)^{12} - \left(\frac{\sigma}{r}\right)^6 - \left(\frac{\sigma}{r_c}\right)^{12} + \left(\frac{\sigma}{r_c}\right)^6\right] & \text{if } r \le r_c \\ 0 & \text{if } r > r_c \end{cases} \tag{3}$$

with $r = r_{ij}$ being the distance between monomers i and j. σ is approximately the diameter of a monomer segment. For an infinitely good solvent, the cutoff distance is taken as $r_c = 2^{1/6}\sigma$, such that the potential is purely repulsive. We refer to this limit of very good solvent condition as the athermal case. In the athermal case, there is no significance to the value of the temperature, and it merely determines the kinetic energy scale. In order to be consistent with our earlier work,[10] we took $T = 1.2\epsilon/k_B$. To introduce the effect of solvent quality, we extended the range of the interaction to $r_c = 2.5\sigma$. Thus by changing T, we could vary the relative importance of the monomer−monomer attraction and change the effective quality of the solvent without explicitly introducing solvent particles. In addition to dendrimers in athermal solvents, we simulated dendrimers at temperatures that correspond to a good solvent ($T = 4.0$), a Θ solvent ($T = 3.0$), and a poor solvent ($T = 2.0$) for linear chains.[11]

The chemical bond between the monomer segments is represented by the attractive potential U^{ch}. The form of this potential is given by

$$U^{ch}(r) = \begin{cases} -0.5kR_0^2\ln[1-(r/R_0)^2] & \text{if } r \le R_0 \\ \infty & \text{if } r > R_0 \end{cases} \tag{4}$$

with $k = (T/1.2)30\epsilon/\sigma^2$ and $R_0 = 1.5\sigma$. r is the distance between a monomer and its neighbors to which it is bonded chemically. This choice of parameters, including the temperature dependence of k, ensures that the average bond length is essentially independent of T and is about 0.97σ.

The equations of motion[12] of the monomers are integrated using a velocity−Verlet algorithm with a time step Δt, taken to be as large as possible, while keeping the integration stable. We used $\Delta t = 0.012\tau$ for the athermal case, and Δt is the range 0.006τ−0.008τ for the cases in which the potential has an extended, attractive contribution. Here $\tau = \sigma(m/\epsilon)^{1/2}$ is the natural time unit in this model. The friction coefficient Γ was set to be $\Gamma = 0.5\tau^{-1}$. We used units in which $m = \sigma = \epsilon = 1$ and measured the temperature in units of ϵ/k_B. Further details on the simulation technique can be found elsewhere.[13]

The initial configuration for the dendrimers in an athermal solvent is built as follows. The stationary core of the dendrimer is taken to be a small sphere of radius 0.5σ. To build the $g = 0$ generation of the dendrimer, b chains of n segments (monomers) are attached at one end onto the core at three randomly chosen points. Here b is the branching factor and n is the number of monomers between each branching point. In the present study, we used $b = 3$ and $n = 7$. The segments of each chain are taken to be nonreversing random walks of length σ. To allow for faster equilibration of the dendrimer, the distance between a newly added monomer and all the previous monomers is constrained to be larger than some r_{min} (constraint of no overlap). If this condition is not fulfilled, a new position is selected for the segment to be inserted. The $g = 1$ generation is built by adding $b - 1$ chains to each of the free ends of the $g = 0$ dendrimer, making sure that the newly added monomers do not overlap with any of the previously added monomers. In the simulations described here, we used $r_{min} = 0.8\sigma$. The same procedure is continued to build dendrimers of higher generation number. Obviously, as g increases, it becomes increasingly difficult to fulfill the constraint of no overlap. If a monomer cannot be inserted after a predetermined number of trials (we used 500 trials), the whole dendrimer is discarded, and the whole process is started again with a new random number seed.

This procedure allowed the construction of the initial configurations of dendrimers up to $g = 6$ within a reasonable computer time. For larger dendrimers, it proved to be practically impossible to fulfill the constraint of no overlap. In order to overcome this problem, we added the monomers for the 7th generation on the free ends of the *equilibrated* $g = 6$ dendrimer. The equilibration was carried out in the manner described

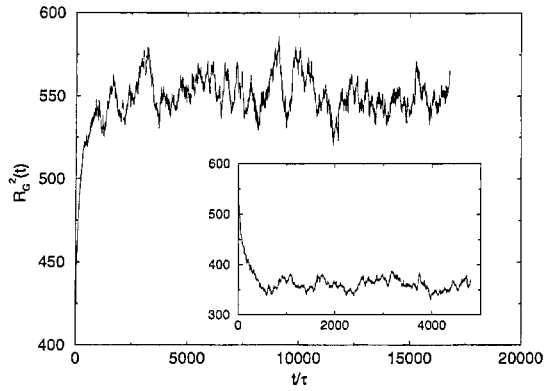

Figure 2. Evolution of the instantaneous R_G^2 of the $g = 8$ dendrimer in an athermal solvent. $t = 0$ corresponds to the nonequilibrium initial configuration. The inset shows the evolution of the instantaneous R_G^2 of the $g = 8$ dendrimer in a good solvent with temperature $T = 4.0$, starting from an equilibrium configuration of the $g = 8$ dendrimer in an athermal solvent.

below. Similarly, the $g = 8$ dendrimer was built from the equilibrated $g = 7$ dendrimer.

In principle, one could build the initial configuration with overlapping monomers, relaxing the constraint of no overlap, and replace the Lennard-Jones potential by a much softer one at the initial stages of the equilibration process, until the monomers are well separated.[10] This approach was used successfully for systems composed of essentially linear chains, such as polymer stars[14,15] and polymer brushes.[16] However, the high level of branching present in the dendrimer system leads to considerable entanglement for the overlapping configuration, and we found it virtually impossible to untie the resulting knots by gradually increasing the magnitude of the repulsive interaction. For small values of the interaction, the overlap of the monomers persisted. When the interaction strength was increased, the small distances between the monomers led to very high local forces, which rendered the simulations unstable.

Starting from the initial configuration, whose construction was described above, the dendrimer in a good solvent was equilibrated. The equilibration was monitored by measuring the overall dimensions of the dendrimer, such as the instantaneous radius of gyration. Figure 2 shows $R_G^2(t)$ of the $g = 8$ dendrimer, with $t = 0$ corresponding to the initial configuration. R_G^2 increases from the value of $425\sigma^2$ at $t = 0$ to about $550\sigma^2$ at equilibrium. The increase from the initial value is rather fast on the time scale shown in the figure; at about $t = 3000\tau$, the equilibrium value is already reached. After that time, R_G^2 fluctuates around the average value, with fluctuations of order $\Delta R_G^2 \simeq 25\sigma^2$. The initial stages of the simulation are excluded from the calculation of the average properties of the dendrimer, such as the radial monomer density distribution. For the $g = 8$ dendrimer, we excluded the first 4800τ from the averages.

Table 1. Details of the Simulations[a]

g	N	T	$\mathcal{T}/\tau$	$\langle R_G^2 \rangle$
8	10731	a.s.	12000	548.0
8	10731	4.0	2400	360.0
8	10731	3.0	4200	260.0
8	10731	2.0	4000	160.0
7	5355	a.s.	12000	375.5
7	5355	4.0	3000	241.7
7	5355	3.0	3500	173.2
7	5355	2.0	4000	101.2
6	2667	a.s.	24000	249.5
6	2667	4.0	6000	154.8
6	2667	3.0	7000	113.8
6	2667	2.0	7000	66.6
5	1323	a.s.	3500	156.2
5	1323	4.0	3500	104.1
5	1323	3.0	4000	75.4
5	1323	2.0	4000	44.1
4	651	a.s.	12000	105.5
3	315	a.s.	12000	63.5
2	147	a.s.	12000	36.2
1	63	a.s.	12000	18.3

[a] g and N are respectively the generation number of the dendrimers and the number of monomers they contain. The solvent quality is indicated by the value of the temperature. "a.s." denotes athermal solvent. The total length of the run after equilibration is reached is denoted by $\mathcal{T}$, in units of τ. $\langle R_G^2 \rangle$ is the mean squared radius of gyration of the equilibrated dendrimer, averaged over the whole sampling run.

The initial configuration of the dendrimers at temperature $T = 4.0$ is taken to be one of the equilibrium configurations of the corresponding dendrimer under athermal solvent conditions (with the repulsive short-range potential). The temperature is changed to $T = 4.0$ and the cutoff of the Lennard-Jones potential is increased to $r_c = 2.5\sigma$, introducing an attractive tail to the potential. The internal structure of the dendrimer responds immediately to these changes, and R_G^2 decreases rapidly. The inset in Figure 2 shows the variation of the R_G^2 with time of the $g = 8$ dendrimer, with the change described above induced at $t = 0$. The

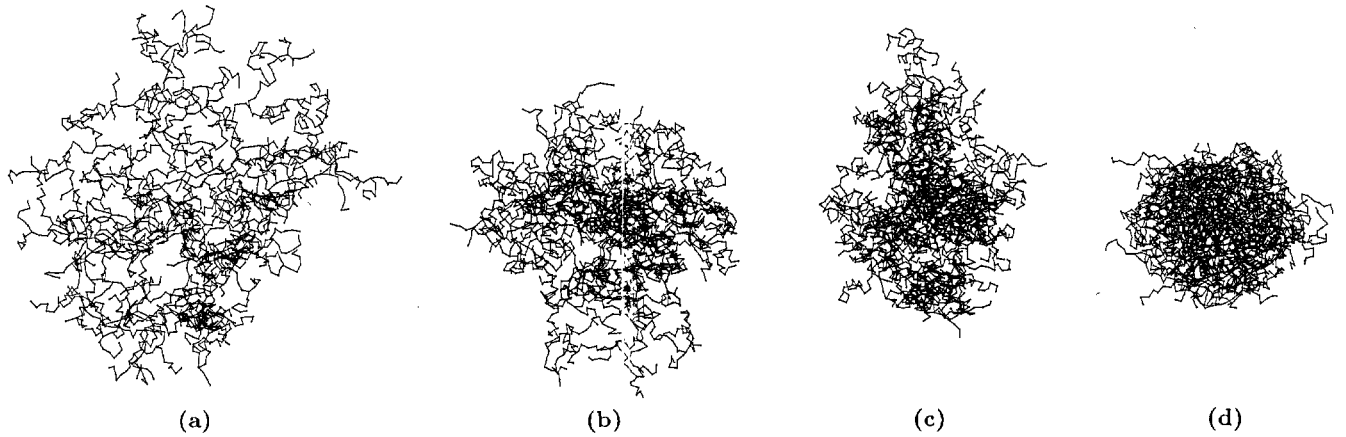

Figure 3. Projections on the $z = 0$ plane of the typical configurations of $g = 6$ dendrimers under various solvent conditions: (a) athermal; (b) $T = 4.0$; (c) $T = 3.0$; (d) $T = 2.0$.

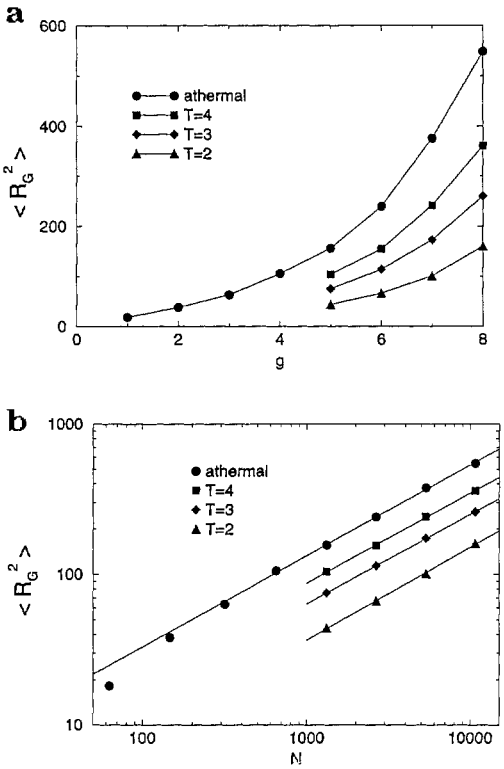

Figure 4. (a) Average mean squared radius of gyration of the dendrimers as a function of the generation number. The different curves correspond to the solvents indicated in the legend. (b) The same quantity as a function of the number of monomers in the dendrimer, on a double-logarithmic scale. The points correspond to the measured averages, while the full lines are best fits of the form $\langle R_G^2 \rangle = AN^x$, calculated using the four highest N values. The slopes are 0.60 for the athermal and $T = 4.0$ cases, 0.59 for $T = 3.0$, and 0.61 for $T = 2.0$.

instantaneous R_G^2 decreases from $550\sigma^2$ to about $360\sigma^2$ in less than 1000τ. Again, the transition stages are not included in the calculation of the average properties. Similarly, the initial configurations of the $T = 3.0$ and $T = 2.0$ dendrimers are taken to be one of the equilibrium configurations of the corresponding $T = 4.0$ and $T = 3.0$ dendrimers, respectively.

In order to check that the equilibration process, as described here, indeed leads to equilibrated structures, we repeated this procedure in the reverse order; that is, we took one of the equilibrium configurations of the $g = 8$, $T = 2.0$ dendrimer, and increased T to 3.0 and calculated the limiting $\langle R_G^2 \rangle$. This value was almost identical to the one obtained by cooling the dendrimer from $T = 4.0$. The warming process was continued to $T = 4.0$ and the good solvent dendrimer. That identical $\langle R_G^2 \rangle$ values were obtained from the two procedures is a clear indication that adequate equilibration of the dendrimers had been achieved.

After reaching equilibrium, we continued the simulations, saving the coordinates of all the monomers to a file every 10 000 time steps. This time difference is long enough so that two consecutive configurations are independent of each other, as will be shown later in section III.F. In addition, we calculated the instantaneous R_G^2 of the dendrimer every 100 time steps, and stored this information and used it to determine the relaxation time τ_R. The dendrimer configurations were also used to calculate average properties. The average monomer density of the dendrimers, $\rho(r)$, is calculated from the configurations by counting the number of monomers whose centers are within a spherical shell

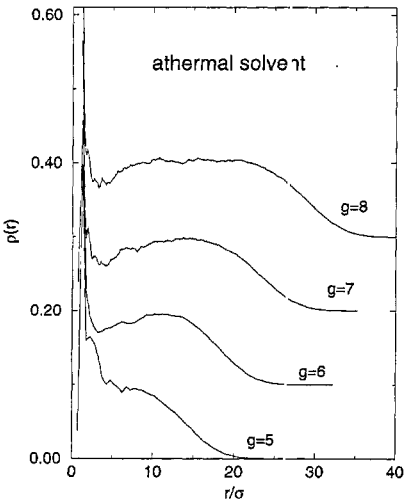

Figure 5. Radial monomer densities of dendrimers in an athermal solvent. The curves for $g = 6$, 7, and 8 are shifted up by 0.1, 0.2, and 0.3, respectively, in the vertical axis for the sake of clarity.

of radius r and thickness Δr. This number, averaged over all the configurations, was divided by the volume of the shell to produce $\rho(r)$. Typically, we used $\Delta r = 0.5\sigma$. Smaller values of Δr give essentially identical, albeit noisier results. Other quantities calculated from the saved configurations will be defined in the next section.

III. Results

The simulations were carried out for dendrimers with $1 \le g \le 8$ under athermal solvent conditions. For the cases where the potential has an attractive tail, simulations were performed for $5 \le g \le 8$. In Table 1 we present our results for the total length of the run after equilibration and the average mean squared radius of gyration of the equilibrated dendrimer for each system studied.

Figure 3 shows planar projections of $g = 6$ dendrimers for each solvent condition studied. One can see that as the solvent quality decreases from the athermal case, via the Θ solvent ($T = 3.0$) to the poor ($T = 2.0$) solvent, the dimensions of the dendrimer shrink, and the density increases. In the rest of this section, we present various quantitative analyses of the equilibrium structure of the dendrimers, based on such equilibrium configurations.

A. Dendrimer Size. The variation of $\langle R_G^2 \rangle$ as a function of the generation number is shown in Figure 4a for all the solvent conditions. Figure 4b shows the same quantity as a function of the number of monomers, N, on a log–log scale. The solid lines are best fits of the form $\langle R_G^2 \rangle = AN^x$, calculated using the points corresponding to $5 \le g \le 8$. The value of x is 0.60 for the athermal case and for $T = 4.0$, 0.59 for $T = 3.0$, and 0.61 for $T = 2.0$. Inverting the relation, we find that for all the cases, $N \propto R_G^{d_f}$, with the fractal dimension $d_f \simeq 3.3$. As the fractal dimension of an object in Euclidian space is limited by the dimensionality of the space, we consider d_f to be 3. Such behavior indicates a compact (i.e., space filling) structure for the dendrimers. This result is consistent with another measure of the "fractal dimension" of dendrimers, based on their density profile, as will be shown below.

B. Radial Density Profile. The monomer number density as a function of the distance from the center, $\rho(r)$, is shown in Figure 5 for dendrimers for the

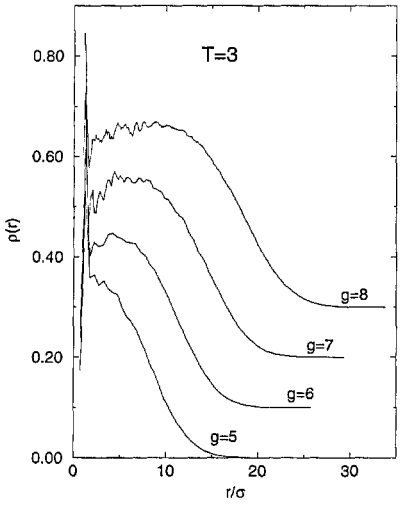

Figure 6. Radial monomer densities of dendrimers in a Θ solvent ($T = 3$). The curves for $g = 6$, 7, and 8 are shifted up by 0.1, 0.2, and 0.3, respectively, in the vertical axis for the sake of clarity.

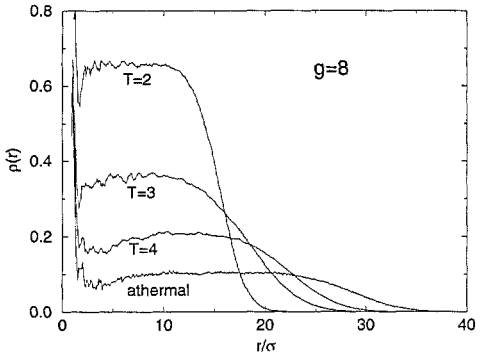

Figure 7. Radial monomer densities of $g = 8$ dendrimers in solvents of varying quality.

athermal case. Curves corresponding to four values of g are depicted. Each curve is shifted from the previous one by 0.1 in the vertical axis, for the sake of clarity. In all the dendrimers, a core region of very high density is apparent near the center. The density rapidly decreases to a local minimum at about $r = 4\sigma$, before increasing to form a region of almost constant density. The constant density zone is most apparent in the $g = 8$ dendrimer where it stretches out to about $r = 25\sigma$. This zone barely exists for the $g = 5$ dendrimer. The constant density region is followed by a tail zone in which the density decreases gradually. The value of the density in this constant density zone is virtually identical for all the dendrimers ($\rho\sigma^2 \simeq 0.1$). The width of the tail zone is also very similar for all the systems.

Similar density profiles are obtained for the finite temperature systems as well. The density profiles shown in Figure 6 for $T = 3.0$ are qualitatively similar to those for the athermal case. The density level at the constant density region is higher ($\rho\sigma^3 \simeq 0.35$) than for the good solvent case, while its width is smaller. This behavior is also observed in Figure 7, in which the density profiles for $g = 8$ dendrimers for the four cases studied are shown. All the curves have similar structure, with the density plateau $\rho\sigma^3 = 0.1$, 0.2, 0.35, and 0.67, respectively.

C. Fractal Structure of the Dendrimers. In a recent paper,[8] Mansfield measured the fractal dimension of the dendrimers using the box method. In this method, one evaluates $M(r)$, which is the number of

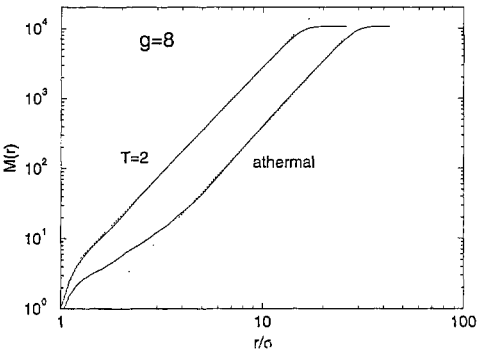

Figure 8. Number of monomers within a sphere of radius r from the center of the dendrimer. The full curves show the average over all the configurations sampled for the $g = 8$ dendrimer for the athermal and poor solvent ($T = 2.0$) cases. The dotted lines are the best power law fits. The slopes of the fits for the athermal and the $T = 2.0$ cases are 3.1 and 3.0, respectively.

monomer segments that reside within a sphere of radius r centered on the center of the dendrimer. He found that the dendrimers at generation numbers $6 \leq g \leq 9$ have a self-similar structure, although the self-similarity extends over a narrow length scale. The fractal dimensions he measured varied between 2.45 and 2.76. This is not consistent with the $N \propto R_G^3$ behavior that is found in the present study. To address this point further, we estimated the "fractal dimension" of the dendrimers in a manner similar to the box method. To that end, we calculated $M(r)$ from the average density profile,

$$M(r) = 4\pi \int_0^r r'^2 \rho(r')\, dr' \qquad (5)$$

Figure 8 shows $M(r)$ for $g = 8$ under both athermal and poor solvent ($T = 2.0$) conditions on a double-logarithmic plot. Also shown are fits of the form $M(r) = Ar^{d_f}$ over the range $5 \leq r/\sigma \leq 25$ for the athermal case and $2 \leq r/\sigma \leq 13$ for the $T = 2.0$ case. The fits, which are very good in this narrow range, give $d_f = 3.1$ and $d_f = 3.0$, respectively, for the two cases. We consider both to be 3 within the accuracy of our simulations. At the tail of the density profile, the integral saturates due to the finite size of the dendrimer. Thus it appears that the dendrimers are compact structures, with a uniform, scale-independent density. The differences in the observed value of the fractal dimension between the present work and that found by Mansfield[8] is probably related to the difficulty in obtaining accurate measures of the fractal dimension when the self-similarity region is narrow. It may also be due to the fact that it is more difficult to relax sufficiently the dense, interior regions of the dendrite in a lattice simulation compared to the present off-lattice simulations.

D. Density Profile of the Generations. How the monomer segments belonging to various generations are distributed within the dendrimer can also be determined in a simulation. We define $\rho_g(r)$ as the monomer density profile due to the segments of generation g. Obviously, the sum over all the $\rho_g(r)$'s at a given point gives the overall density at that point. Parts a and b of Figure 9 show the various contributions for $g_{max} = 8$ and $g_{max} = 6$ dendrimers, respectively, under athermal conditions. The various contributions for a $g_{max} = 8$ dendrimer in a poor ($T = 2.0$) solvent are shown in Figure 9c. (In this subsection, we use g_{max} to denote the generation number of the dendrimer, while g indicates the individual

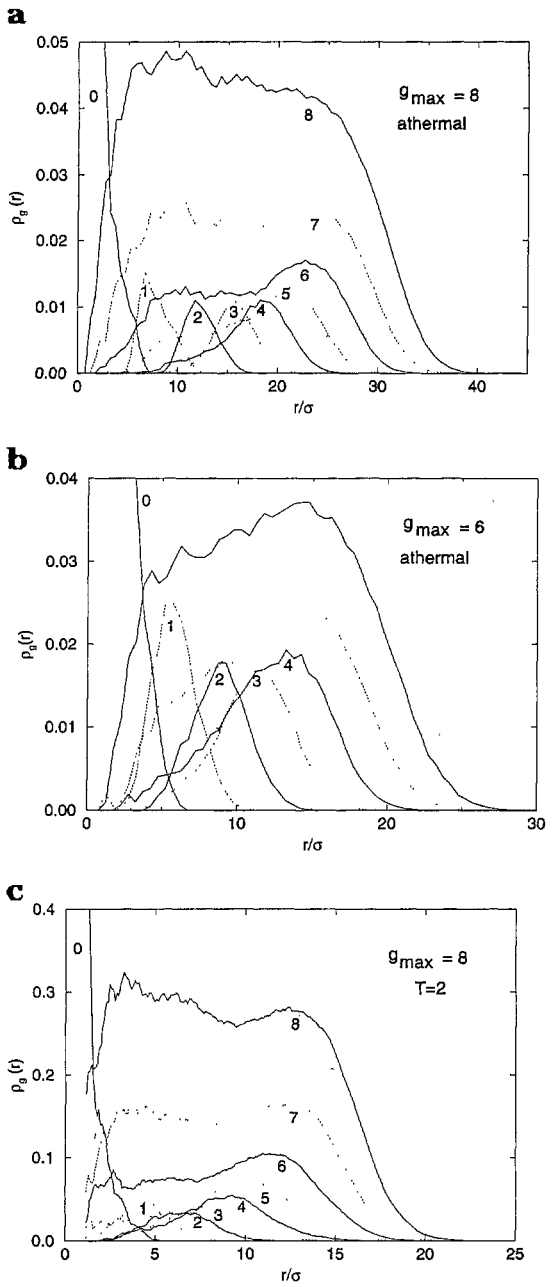

Figure 9. Contributions to the overall monomer density profile, due to monomers of the generation g, for a dendrimer of generation number g_{max}: (a) $g_{max} = 8$, athermal solvent; (b) $g_{max} = 6$, athermal solvent; (c) $g_{max} = 8$, $T = 2.0$.

generations within the dendrimer.) In all the cases, it is seen that the monomers belonging to generations 0 $\leq g \leq 4$ are fairly localized, with the peak of their density profiles moving farther away from the core with increasing g. Mansfield and Klushin[7] came to a similar conclusion that the segments of the earlier generations are extended, by measuring the fraction of bonds with trans configuration as a function of the generation number. We also see that the overlap between the different ρ_g's is low for the earlier generations and becomes appreciable as g increases. At $g = 5$, an additional shoulder is formed at lower values of r, indicating that these monomers penetrate into the interior of the dendrimer. At higher generations, the density at the interior increases, until at $g = g_{max}$, the density is almost uniform over the whole r range. (Most of the monomers are still at the outermost regions, as the number of monomers at a distance r is obtained by multiplying the density by $4\pi r^2$.) In particular, the density due to the terminal generation is completely mobile, with an approximately uniform density everywhere in the dendrimer, down to the core regions, where even monomers of the inner generations are excluded.

Comparing Figure 9a with Figure 9b, we see that for the $g_{max} = 6$ dendrimer, the peaks of the density profile of the lower generations occur at a lower distance from the center than for the ρ_g of the corresponding generation of the $g_{max} = 8$ dendrimer. This is probably due to the fact that in a $g_{max} = 8$ dendrimer, there are more monomer segments of the higher generations penetrating into the interior of the dendrimer, forcing the monomers of the earlier generations to extend further. From Figure 9c, which corresponds to a $g_{max} = 8$ dendrimer under poor solvent conditions, one sees a picture qualitatively similar to the one seen for the same dendrimer under athermal conditions, except that the density profiles extend to smaller distances, resulting from the poor affinity of the monomer to the solvent.

E. Segregation of the Dendrons. Mansfield[8] first noted that the segments belonging to the three major dendrons (the three branches formed at the initial branching) tend to segregate. The segregation is evident both in a single configuration and in the time-averaged projection of the dendrimer. He gave evidence of segregation at secondary levels of branching as well.

Segregation of the dendrons is observed in our simulations as well. From three-dimensional snapshots of the dendrites, the spatial segregation of the dendrons is apparent as found by Mansfield.[8] In order to quantify the amount of segregation and to study its dependence on various parameters, we divided the space around the center of the dendrimer into cubic cells of length σ and defined $\psi_b(i,j,k)$ to be the average number of monomers that belong to branch b, which are inside the cell identified by the indices i, j, and k. The average is over all the different configurations of the dendrimer, taken during the sampling run. From this we define the total overlap $\mathcal{O}_t$ as

$$\mathcal{O}_t = \frac{\sum_{\{i,j,k\}} (\psi_1\psi_2 + \psi_2\psi_3 + \psi_3\psi_1)}{\sum_{\{i,j,k\}} (\psi_1^2 + \psi_2^2 + \psi_3^2)} \qquad (6)$$

Here the sum is over all the cells that are part of the dendrimer, and $\psi_b \equiv \psi_b(i,j,k)$. If the branches are completely segregated, a cell will be populated by monomers belonging to only one branch, so that only one of the three ψ_b's at that cell will be nonzero. This will give a vanishing total overlap. If, on the other hand, the three branches are totally mixed, the three ψ_b's at each cell will have identical values, leading to $\mathcal{O}_t = 1$. Figure 10 shows the $\mathcal{O}_t$ values calculated for the different dendrimers studied. The amount of overlap increases with decreasing solvent quality. This is expected,[8] as the dendrimer becomes denser with decreasing solvent quality.

Mansfield has recently conjectured[8] that at the terminal generation number, where it would be impossible to insert any more monomers, the dendrons should intermix. The trend seen in Figure 10, that for given solvent quality, the amount of overlap decreases with increasing generation number, does not support this conjecture. Another trend observed in Figure 10 is that the differences in the total overlap for solvents of

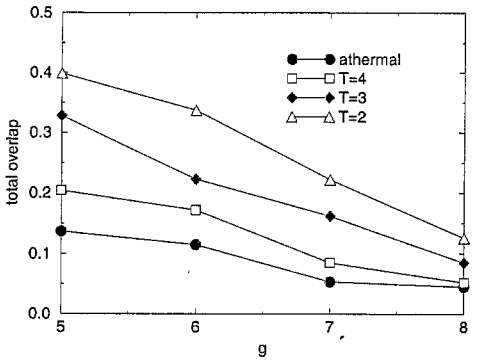

Figure 10. Total overlap between the different dendrons, as defined in eq 6, for dendrimers with $5 \le g \le 8$, under different solvent conditions.

different quality seem to decrease as the generation number increases.

A different, more local measure of segregation is given by $O(r)$, which is the average overlap at the radial distance r from the dendrimer center. We define $O(r)$ for discrete values of r/σ as

$$O(r) = \frac{\sum_{\{i,j,k\}} (\psi_1\psi_2 + \psi_2\psi_3 + \psi_3\psi_1)\delta_{r,r_{i,j,k}}}{\sum_{i,j,k} (\psi_1^2 + \psi_2^2 + \psi_3^2)\delta_{r,r_{i,j,k}}} \quad (7)$$

That is, the sum is over only those cells that are in the spherical shell between r/σ and $r/\sigma + 1$. In principle, it is possible to define $O(r)$ for continuous values of r; however, evaluating the sum over thinner shells leads to larger fluctuations in $O(r)$. We evaluate $O(r)$ only for those values of r/σ for which the denominator in eq 7 is not zero; that is, the monomer density is finite. This function is shown in Figure 11a for dendrimers with $g = 4$, 6, and 8 under good solvent conditions and in Figure 11b for dendrimers with $g = 6$ under different solvent conditions. In both plots, the radial distance is divided by the corresponding average $\langle R_G^2\rangle^{1/2}$. $O(r)$ is of order 1 only at the core region ($r/\sigma < 1$), after which it drops abruptly. For the good solvent case, the drop is to about 0.2. As the solvent quality worsens, the drop is less significant. After the drop, $O(r)$ decays gradually to 0. In this region of gradual decay, the value of the local overlap is higher (for a given $r/\langle R_G^2\rangle^{1/2}$) for the smaller dendrimer and for the lower solvent conditions. This behavior is consistent with the behavior found for the total overlap.

F. Relaxation of the Internal Structure. Up to now, we have discussed the static properties of the dendrimers. The dynamic properties of polymeric systems in general and of dendrimers in particular are also of interest. In this study, we have mainly been interested in the relaxation of the dendrimer from one equilibrium configuration into another completely independent one. Our interest in partially motivated by the question whether the simulations are long enough and give enough independent configurations for sufficient averaging of the static properties. A convenient measure of the relaxation is determined from the decay of the autocorrelation function,

$$C(t) = \frac{\langle (X(t) - X_{av})(X(0) - X_{av})\rangle}{\langle X^2\rangle_{av} - X_{av}^2} \quad (8)$$

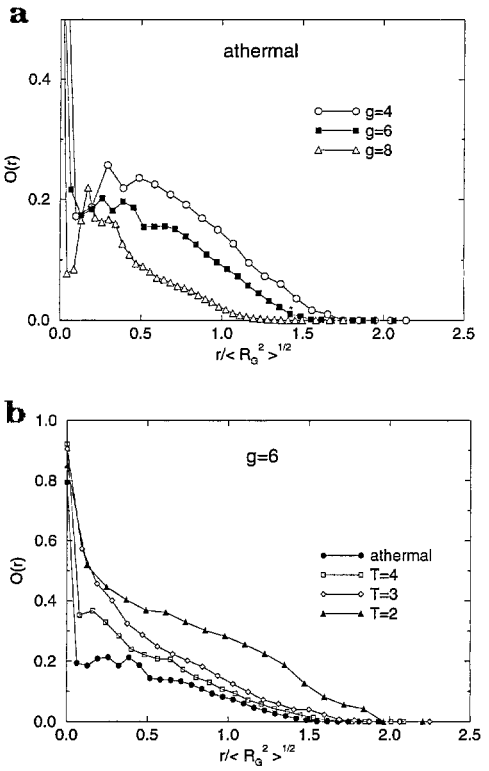

Figure 11. Overlap between the different dendrons, at a given distance from the center, as defined in eq 7. The radial distance is scaled by $\langle R_G^2\rangle^{1/2}$ of the dendrimer. (a) $O(r)$ for dendrimers with $g = 4$, 6, and 8 under athermal solvent conditions. (b) $O(r)$ for dendrimers with $g = 6$ under different solvent conditions.

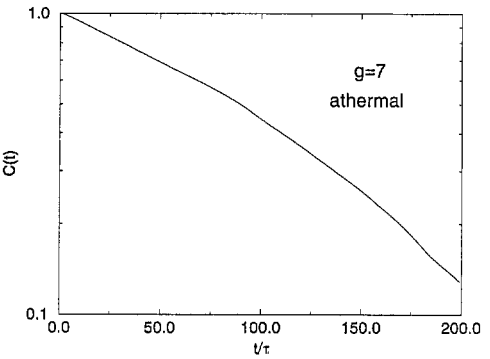

Figure 12. Autocorrelation function of $R_G^2(t)$ for $g = 7$ and athermal conditions.

Here $X(t)$ is the instantaneous value of some property of the dendrimers. We have calculated $C(t)$ for $X(t) = R_G^2(t)$, to estimate the relaxation time. A typical $C(t)$ behavior is shown in Figure 12 for the $g = 7$ dendrimer in an athermal solvent. The relaxation time τ_R is estimated from this curve either from the long-time slope on a semilogarithmic plot or from using $C(\tau_R) = 1/e$. Although there are more elaborate methods of estimating the relaxation time,[17] our investigation of the dynamic behavior has not been detailed enough to justify such methods.

The relaxation time obtained from Figure 12 for $g = 7$ is about 130τ, much smaller than the length of the sampling run used for the same dendrimer, about 12000τ. For the other cases studied, we verified that the sampling runs were indeed much longer than the relaxation times. We also tried to make a systematic study of the dependence of the relaxation time on the generation number and the solvent quality. The relax-

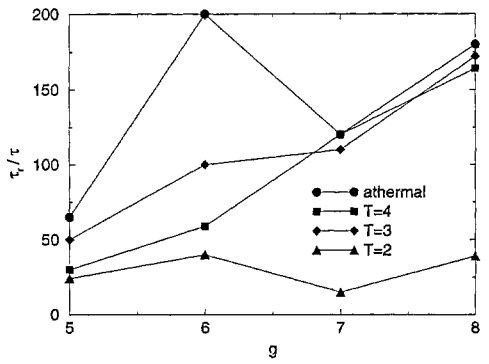

Figure 13. Relaxation time derived from the decay of $C(t)$ as a function of the generation number for dendrimers under various solvent conditions.

ation times calculated in a manner described above are shown in Figure 13. Although one cannot derive from the results a quantitative dependence, it seems that the relaxation time increases with increasing g and solvent quality. It is not clear why the dependence of τ_R on g is noisy. It may be due to the fact that good estimates of the relaxation time requires very long sampling runs. Another possible reason is that due to the high densities reached near the dendrimer core and the high levels of branching, there are entanglements, leading to very slow disentanglement processes.

IV. Conclusion

We have presented a molecular dynamics study of a coarse-grained model of dendrimers under various solvent conditions. The molecular dynamics method has proven to be quite efficient in simulating the equilibrium structure of the dendrimers.

The density profile of the dendrimers at all solvent conditions exhibits a high-density region near the central core, a plateau region, and a local minimum between them. Beyond the plateau region, the density drops slowly. The density at the plateau is independent of the generation number and increases with decreasing solvent quality. The length of the plateau region, on the other hand, increases with increasing generation number.

The size of the dendrimer, as measured by its radius of gyration, increases roughly as $N^{1/3}$, with N being the number of monomers the dendrimer contains. This indicates a compact structure, with a fractal dimensionality of 3. This result holds for all solvent conditions. Evaluation of the fractal dimension by the method of box counting also gives the same result. Our result does not agree with that of Lescanec and Muthukumar[5] ($R \propto N^{0.22}$) nor with the box counting estimate of Mansfield[8] for the fractal dimension (2.45–2.76 for generation numbers of 6–9).

By evaluating the monomer density for each generation, we have shown that the monomers belonging to the early generations are localized within a narrow radial range, with little overlap of the density profiles due to these generations. The chain segments belonging to these generations are radially stretched. However, starting from the fifth generation for the case $n = 7$ studied here, significant backfolding occurs. The amount of backfolding increases for the later generations to such an extent that the monomers of the last generation penetrate all regions of the dendrimer, including the core region. This result is consistent with similar conclusions reached by previous studies.[5,7]

Similar to the observation by Mansfield,[8] we have also observed segregation of the dendrons. By quantifying the amount of dendron overlap using two measures of overlap, we have shown that the amount of dendron overlap increases with decreasing solvent quality; that is, the dendrons segregate less when the solvent is poorer. For fixed solvent quality, the amount of dendron overlap decreases with increasing generation number.

We have also evaluated the relaxation times of the autocorrelation functions of the temporal fluctuations of the squared radius of gyration of the dendrimers. Our motivation has been to ensure that adequate sampling was performed for the calculation of the equilibrium properties. Our estimates of the relaxation times are not of high enough quality to obtain the dependence of the relaxation times on the generation number and the solvent quality. It appears that the fluctuation of the internal structure of the dendrimers is a complex process that cannot be characterized by a single relaxation time.

References and Notes

(1) Tomalia, D. A.; Baker, H.; Dewald, J. R.; Hall, M.; Kallos, G.; Martin, S.; Roeck, J.; Ryder, J.; Smith, P. *Polym. J. (Tokyo)* **1985**, *17*, 117. Tomalia, D. A.; Baker, H.; Dewald, J. R.; Hall, M.; Kallos, G.; Martin, S.; Roeck, J.; Ryder, J.; Smith, P. *Macromolecules* **1986**, *19*, 2466.
(2) Voit, B. I. *Acta Polym.* **1995**, *46*, 87.
(3) de Gennes, P.-G.; Hervet, H. *J. Phys. Lett. Fr.* **1983**, *44*, L351.
(4) Naylor, A. M.; Goddard, W. A., III; Kiefer, G. E.; Tomalia, D. A. *J. Am. Chem. Soc.* **1989**, *111*, 2339.
(5) Lescanec, R. L.; Muthukumar, M. *Macromolecules* **1990**, *23*, 2280.
(6) Mansfield, M. L.; Klushin, L. I. *J. Phys. Chem.* **1992**, *96*, 3994.
(7) Mansfield, M. L.; Klushin, L. I. *Macromolecules* **1993**, *26*, 4262.
(8) Mansfield, M. L. *Polymer* **1994**, *35*, 1827.
(9) Biswas, P.; Cherayil, B. J. *J. Chem. Phys.* **1994**, *100*, 3201.
(10) Grest, G. S.; Murat, M. In *Monte Carlo and Molecular Dynamics Simulations in Polymer Science*, Binder, K., Ed.; Oxford University Press: New York, 1995; p 476.
(11) Grest, G. S.; Murat, M. *Macromolecules* **1993**, *26*, 3108.
(12) Allen, M. P.; Tildesley, D. J. *Computer Simulation of Liquids*; Clarendon: Oxford, 1987.
(13) Grest, G. S.; Dünweg, B.; Kremer, K. *Comput. Phys. Commun.* **1989**, *55*, 269.
(14) Grest, G. S.; Kremer, K.; Witten, T. A. *Macromolecules* **1987**, *20*, 1376.
(15) Grest, G. S.; Kremer, K.; Milner, S. T.; Witten, T. A. *Macromolecules* **1989**, *22*, 1904.
(16) Murat, M.; Grest, G. S. *Macromolecules* **1989**, *22*, 4054.
(17) Neelov, I. M.; Binder, K. *Macromol. Theory Simul.* **1995**, *4*, 1063.

MA951219E